NASA/TM–2013-218027

Iodine Tagging Velocimetry and Mechanism in the Hypersonic Near Wake of a MultiPurpose Crew Vehicle

R. Jeffrey Balla
Langley Research Center, Hampton, Virginia

July 2013

NASA STI Program . . . in Profile

Since its founding, NASA has been dedicated to the advancement of aeronautics and space science. The NASA scientific and technical information (STI) program plays a key part in helping NASA maintain this important role.

The NASA STI program operates under the auspices of the Agency Chief Information Officer. It collects, organizes, provides for archiving, and disseminates NASA's STI. The NASA STI program provides access to the NASA Aeronautics and Space Database and its public interface, the NASA Technical Report Server, thus providing one of the largest collections of aeronautical and space science STI in the world. Results are published in both non-NASA channels and by NASA in the NASA STI Report Series, which includes the following report types:

- TECHNICAL PUBLICATION. Reports of completed research or a major significant phase of research that present the results of NASA Programs and include extensive data or theoretical analysis. Includes compilations of significant scientific and technical data and information deemed to be of continuing reference value. NASA counterpart of peer-reviewed formal professional papers, but having less stringent limitations on manuscript length and extent of graphic presentations.

- TECHNICAL MEMORANDUM. Scientific and technical findings that are preliminary or of specialized interest, e.g., quick release reports, working papers, and bibliographies that contain minimal annotation. Does not contain extensive analysis.

- CONTRACTOR REPORT. Scientific and technical findings by NASA-sponsored contractors and grantees.

- CONFERENCE PUBLICATION. Collected papers from scientific and technical conferences, symposia, seminars, or other meetings sponsored or co-sponsored by NASA.

- SPECIAL PUBLICATION. Scientific, technical, or historical information from NASA programs, projects, and missions, often concerned with subjects having substantial public interest.

- TECHNICAL TRANSLATION. English-language translations of foreign scientific and technical material pertinent to NASA's mission.

Specialized services also include organizing and publishing research results, distributing specialized research announcements and feeds, providing information desk and personal search support, and enabling data exchange services.

For more information about the NASA STI program, see the following:

- Access the NASA STI program home page at *http://www.sti.nasa.gov*

- E-mail your question to help@sti.nasa.gov

- Fax your question to the NASA STI Information Desk at 443-757-5803

- Phone the NASA STI Information Desk at 443-757-5802

- Write to:
  STI Information Desk
  NASA Center for AeroSpace Information
  7115 Standard Drive
  Hanover, MD 21076-1320

NASA/TM–2013-218027

Iodine Tagging Velocimetry and Mechanism in the Hypersonic Near Wake of a MultiPurpose Crew Vehicle

R. Jeffrey Balla
Langley Research Center, Hampton, Virginia

National Aeronautics and
Space Administration

Langley Research Center
Hampton, Virginia 23681-2199

July 2013

Available from:

NASA Center for AeroSpace Information
7115 Standard Drive
Hanover, MD 21076-1320
443-757-5802

Iodine Tagging Velocimetry and Mechanism in the Hypersonic Near Wake of a MultiPurpose Crew Vehicle

R. Jeffrey Balla[1]
NASA Langley Research Center

[1] Senior Research Scientist, Advanced Sensing and Optical Measurement Branch, MS 493, Adjunct Professor, Physics Dept., Old Dominion University, email:robert.j.balla@nasa.gov
Senior member AIAA

Abstract

This study demonstrates a new molecular tagging velocimetry(MTV) method for velocity measurements of high speed flow. It demonstrates offbody Iodine Tagging Velocimetry (ITV) in the hypersonic near wake of a MultiPurpose Crew Vehicle(MPCV) model. Experiments are performed in the NASA-Langley 31-inch Mach 10 air wind tunnel. A 0.5% I_2 / N_2 mixture is seeded on the leeward backshell of the model using a pressure tap. I_2 laser-induced fluorescence is excited along a 5.5 mm line using an ArF excimer laser near 193 nm. Results indicate I_2 absorbs at least 2 photons to produce iodine ions and electrons. These recombine as the tagged region is displaced downstream to produce I ($^2P_{3/2}$) whose emission is monitored at 206 nm. Results at P_0 = 2.41 MPa (350 psi), T_0 = 990K, and 10 µsec transit times produce velocities from 630-820 m/sec across the I_2 seeded jet at a distance of 38.2 mm (25.5 jet diameters) downstream from the jet orifice. Maximum wake jet velocities near the shear layer are 59% of freestream velocity.

I. Introduction

This study represents the third in a series of articles developing new instrumentation to measure offbody parameters in the freestream, bowshock, and wakes of models in a Mach 10 air windtunnel. Here effort is directed towards velocity measurements in near and far hypersonic wakes. These wakes can be highly three dimensional, contain densities of 0.03–3.0 x 10^{17} cm^{-3}, and contain a variety of issues including flow separation and reversal, unsteady conditions, shear layers, jets for reaction control systems, and high velocity gradients. Current instrumentation is inadequate. The result is a lack of data for computational comparison and limited understanding of the fundamental flow physics. Decadal reviews of freestream and model flowfield instrumentation have been performed in 1992 [1], 1998 [2], and 2009 [3].

It is well known that current surface methods are indirectly measuring off-body flow features which determine many flow field characteristics. New wake instrumentation must be capable of quantitative spatially-resolved nonintrusive

molecular-based and of highest importance offbody measurements at a point, along a line, and preferably in a plane. Specific problems of interest as well as problems with adapting traditional quantitative subsonic offbody instrumentation to hypersonic wake flows have been discussed [4]. Methods include Schlieren, Pitot tubes, hot-wire anemometry, and particle methods such as LDV and PIV. All encounter significant problems in the low densities, high velocity gradients, and complex flow interactions in hypersonic wakes. Most are intrusive and disturb the flow being investigated.

A large number of molecular diagnostic methods are potentially applicable to hypersonic wakes. Even a brief discussion of all potential methods let alone their subtle variations is beyond the scope of this article. This section concentrates on select methods which have been demonstrated or the author concludes might be adapted to provide *quantitative* offbody measurements of velocity in a hypersonic electrically-heated air wake along with their potential advantages and disadvantages. Since the primary interest is viability, no consideration is given to quantitative errors. Since the test fluid is air at temperatures near or below 300K, diagnostics should be designed around atomic or molecular seeds which are chemically nonreactive and do not require a heated carrier gas.

Sodium-based laser-induced fluorescence(LIF) [5] was used to measure velocity, temperature and pressure in hypersonic helium. Sodium is useful for nitrogen or other inert-gas flows. However, it must be injected with a heated carrier gas, reacts explosively with water vapor, and forms oxides in dry air. The resulting heat can perturb the flow.

Raman Doppler Velocimetry can measure velocity, temperature, and pressure [6]. RDV is possible in a hypersonic wake but requires a complex multilaser setup. Expected low signal-to-noise(S/N) ratio would make this a difficult measurement.

Velocimetry using RELIEF has the advantage of vibrationally excited oxygen with a millisecond lifetime [7]. This is compared to typical molecular tagging velocimetry (MTV) methods using diatomics such as nitric oxide (NO) which has a 220 ns natural fluorescence lifetime. This allows longer transits between excitation and interrogation times resulting in potentially higher accuracy for constant velocity flows. RELIEF is currently limited to less than ~700K and greater than ~0.1 Amagat [8]. A RELIEF measurement in a 0.001 Amagat (1 Torr) air wake would be challenging.

The MTV approach is an effective method for offbody velocimetry measurements. It uses a single laser to tag a molecular species of interest and a single camera to measure fluid displacement using LIF between two locations along with transit time. A review of this approach along with its many variations has been presented [9].

APART is an MTV method which locally creates NO fluorescence using a focused ArF excimer in air [10]. This method provides velocimetry with no seeding requirement. Since ground-electronic-state NO is produced continually by a chemical reaction, laser-induced fluorescence has been observed using a probe laser up to 1 sec after the ArF excimer pulse. Neither APART nor RELIEF can be used in hypersonic and impulse facilities using pure nitrogen.

Low wake densities combined with a lack of effective diagnostics based on nitrogen or oxygen dictate flow seeding. Since trace seeding is required to minimize

flow perturbations, the only sufficiently sensitive detection method capable of spatially-resolved instantaneous measurements is LIF. LIF cross sections are typically 10^3 larger than Rayleigh cross sections [11], produce high signals, and offer the potential for planar measurements. Filters effectively separate fluorescence from scattered light. Measurements near and on model surfaces are possible. Flow field perturbation can be studied using active and passive seeding methods. Quantum-state-specific chemical and vibrational nonequilibrium can be measured and compared with computational results. Most are based on nitric oxide planar laser-induced fluorescence (NO PLIF). NO is corrosive and a toxic gas with a threshold limit value of 25 ppm.

Several NO PLIF-based methods have measured velocity in the T2 free-piston shock tunnel at the Australian National University. MTV was used to measure the velocity profile in a Mach 8.5 laminar, hypersonic boundary layer [12]. Two components of velocity were measured in an axisymmetric hypersonic near-wake flow field around a model planetary entry vehicle configuration using Doppler shifts [13]. Shapes and positions of NO spectral lines at every location in the flow are determined using successive T2 runs. Since a single laser shot is acquired during each 300 μsec run, this approach requires high facility run-to-run reproducibility.

NO PLIF-based MTV has been demonstrated in a pure nitrogen jet in the wake of a CEV model in the NASA Langley 31-inch Mach 10 air wind tunnel [14]. Simultaneous multiple velocity profiles were obtained using sequentially-imaged fluorescence tagging. One advantage of this method is its simplicity and the use of a single laser and camera. This method suffers from a short excited state lifetime (< 220 ns) which is further reduced by oxygen quenching. This limits transit times, increases uncertainties, and dictates high-speed applications.

Visible I_2 LIF diagnostics using the B $^3\Pi^+_{ou} \leftarrow$ X $^1\Sigma^+_g$ transition near 514.5 nm have been reviewed[15]. This method has seen considerable development and broad application in a variety of subsonic and supersonic flows. It has demonstrated combined density, temperature, and velocity [16] along with planar velocity and pressure[17]. Time-averaged values of velocity and temperature have been measured in an I_2-seeded N_2 hypersonic free jet facility at Mach 12 using hyperfine transitions. Unfortunately, the time required for these scans is greater than the run time of most full-scale facilities [18]. To overcome corrosion problems associated with large quantities of I_2 filling the entire flow, McDaniel et al. [19] constructed an aluminum wind tunnel painted with flat-black paint along with gaskets and o-ring seals made of Viton for I_2 compatibility. Chemical reactivity and toxicity issues connected with large quantities of seeded I_2 combined with facility redesign and recertification for appropriate gaskets make this approach unsuitable for typical large-scale wind tunnels.

The ultraviolet iodine laser–induced fluorescence (UV I_2 LIF) diagnostic uses the Cordes band $D^1\sum^+_u \leftarrow X\ 1\sum^+_g$ transitions near 193 nm. It was developed by LaRC researchers specifically for hypersonic wakes. UV cross sections are 30x greater than visible cross sections and do not suffer from predissocation. I_2 ion-pair unquenchable excited states produce fluorescence quantum yields of 1 even at atmospheric pressure [20]. Both passive[21] and active[4] seeding are possible. Compared to visible I_2 LIF, this approach provides higher signals with lower seed densities. The result is diagnostics well suited for low-density wake measurements.

Using local seeding of trace quantities of iodine, traditional problems with iodine facility corrosion and toxicity are minimized. Planar flow visualization of 3 x 10^{12} cm^{-3} iodine in a Mach 6 wake with 1.8 x 10^{17} cm^{-3} air was demonstrated using a right circular cylinder[21]. Previous studies have demonstrated density [22] and temperature [23] in the laboratory along with a discussion of the spectroscopy involved.

The problem of hypersonic wake time-of-flight velocimetry has been one of finding a seed species with sufficiently long fluorescence or chemical lifetime. Assuming wake velocities are ½ the freestream velocity, velocities across the wake shear layer range from 300-800 m/sec. These values are in agreement with experiments [14] and CFD computations [14,24]. Assuming a goal of 1% error spanning 100 CCD pixels, transit times of ~10 μsec are required. Typically, molecular species are selected. Atomic species are considered unfeasible for time-of-flight velocimetry since emission lifetimes are typically < 50 ns [25]. Atom velocimetry has been demonstrated using Doppler shifts in arc jets with atomic hydrogen [26] or atomic copper [27]. Another approach used a pump laser to create Laser-Enhanced Ionization(LEI) of either sodium in a shock tube [28] or strontium ions in a flame [29] followed by a probe laser to generate laser-induced fluorescence with appropriate delay.

O'Keefe et al. [30] have shown it is possible to form high-n Rydberg atoms of iodine by resonant two-photon excitation of molecular iodine using an ArF excimer laser. Results suggest I_2 absorbs 2 photons to produce a molecular Rydberg state of I_2*[R($B^2\sum^+_g$)] in a super-excited state(SES). These converge on the I_2^+ ($B\ ^2\sum^+_g$) state of the ion. The SES predissociates into ground state I($^2P^0_{3/2}$) and a high-n Rydberg iodine atom I* [R^3P_2)] with an average Rydberg lifetime of 325 ± 25 μsec lifetime in a zero kinetic energy (ZEKE) state.

Mills et al. [31] proposed that lifetime limitations associated with atomic species might be overcome using high-n Rydberg iodine atom I* [R^3P_2)] or any similar atomic species produced by the mechanism described by O'Keefe et al. [30]. Based on calculations of expected signal levels, Mills et al. [31] also proposed using a noble gas(krypton $4p^5\ 5s^1$ $[3/2]_2$ state) metastable state created by two-photon ArF excimer laser excitation.

Although I_2 is 8.8x heavier than air, velocity lag or slip is negligible in N_2-based flows up to Mach numbers < 5 since velocity is equilibrated within ~ 10 collisions [15]. Hence no velocity lag is expected for atomic or molecular iodine under the conditions of this experiment.

Efforts are directed toward the development of wake instrumentation for the Langley Aerothermodynamic Labs and the 31-inch Mach 10 air wind tunnel in particular. Previously, laser Rayleigh scattering was used to measure freestream densities [32]. UV I_2 LIF was used to measure density [4] of a jet along a line in the wake. The original goal of the present study was to explore the concept of Mills et al[31] to use two photon excitation of I_2 for the production of high-n Rydberg atoms and subsequent velocimetry. Serendipitously an alternate iodine-based energy-storage mechanism was discovered allowing hypersonic wake velocimetry. Iodine is locally seeded from a pressure port in the wake of a CEV model in a Mach 10 flow field. Iodine velocity results are compared

to previous NO PLIF measurements and CFD computations in the 31-inch Mach 10 facility [14,24].

II. Experimental

Complete descriptions of various components of the experimental setup including the iodine seeding procedure, laser configuration, and CCD camera detector have been presented [4,32]. A brief synopsis of previous setups is presented along with a complete description of new additions.

Experiments are performed during Test 466 in the NASA Langley 31-Inch Mach 10 (31M10) Air Tunnel. It is a unique 12.5-MW electrically-heated blowdown-mode facility [33]. The test gas is air which is dried using an activated alumina dryer which provides a dewpoint temperature of 232.4 K (- 41 °F) at a pressure of 4.137 MPa (600 psi). Air is expanded using a three-dimensional contoured nozzle to minimize centerline disturbances characteristic of axisymmetric contoured nozzles. The result is a highly uniform core flow. The test section is 78.7 cm square. Core flow is 25% of the test section, or ± 10 cm about the centerline at low stagnation pressures(P_o = 350 psi) and increases ± 15 cm as the tunnel wall boundary layer thins at high pressures(P_o = 1450 psi).

Optical access is provided by three uncoated Corning 7980 windows with transmission > 85% at 193 nm. These form three orthogonal walls of the test section. Models are positioned on the facility centerline in less than 0.6 seconds using a hydraulically-operated injection system mounted on the rear sidewall.

Facility test times are ~ 60 seconds. The facility typically operates at a single stagnation reservoir temperature T_o = 1,000K (1,350 °F) to prevent air liquefaction. Facility stagnation reservoir pressure P_o was maintained at 2.41 MPa (350 psia). Flow conditions were computed assuming isentropic expansion.

The experimental setup for line measurements along a laser beam is shown in Fig. 1 using ViDI [34]. ViDI is a Langley software tool for interactive 3-D display of the facility, test article, data, and computational fluid dynamics prediction. All details of the 31M10 facility, UV iodine line and LIF (UV I2 LIF) optical setup, sting, strut, and MPCV test article are modeled and presented. This allows the experiment to be constructed, tested, and refined in a virtual environment before facility testing. The constraints of two days of facility setup time and a single day for testing dictated an easy-transport rapid-setup light source. A low-pulse-energy Lambda Physik OpTexPro excimer laser operating on argon-fluoride near 193 nm was selected. The output passes through ~ 1 m of air before it enters the facility. It is turned 90 deg with a mirror and focused into the I_2 jet 38.2 mm (25.5 jet diameters) downstream from the I_2 jet exit (port 4) using an uncoated 600 mm focal length Suprasil lens. Focused laser energy is 2.5 mJ, focal spot size is ~200 μm, and Rayleigh length is ~ 65 cm. Laser alignment assumes the I_2 jet comes straight back off the model with minimal curvature in a plane normal to the freestream flow near the center of the facility.

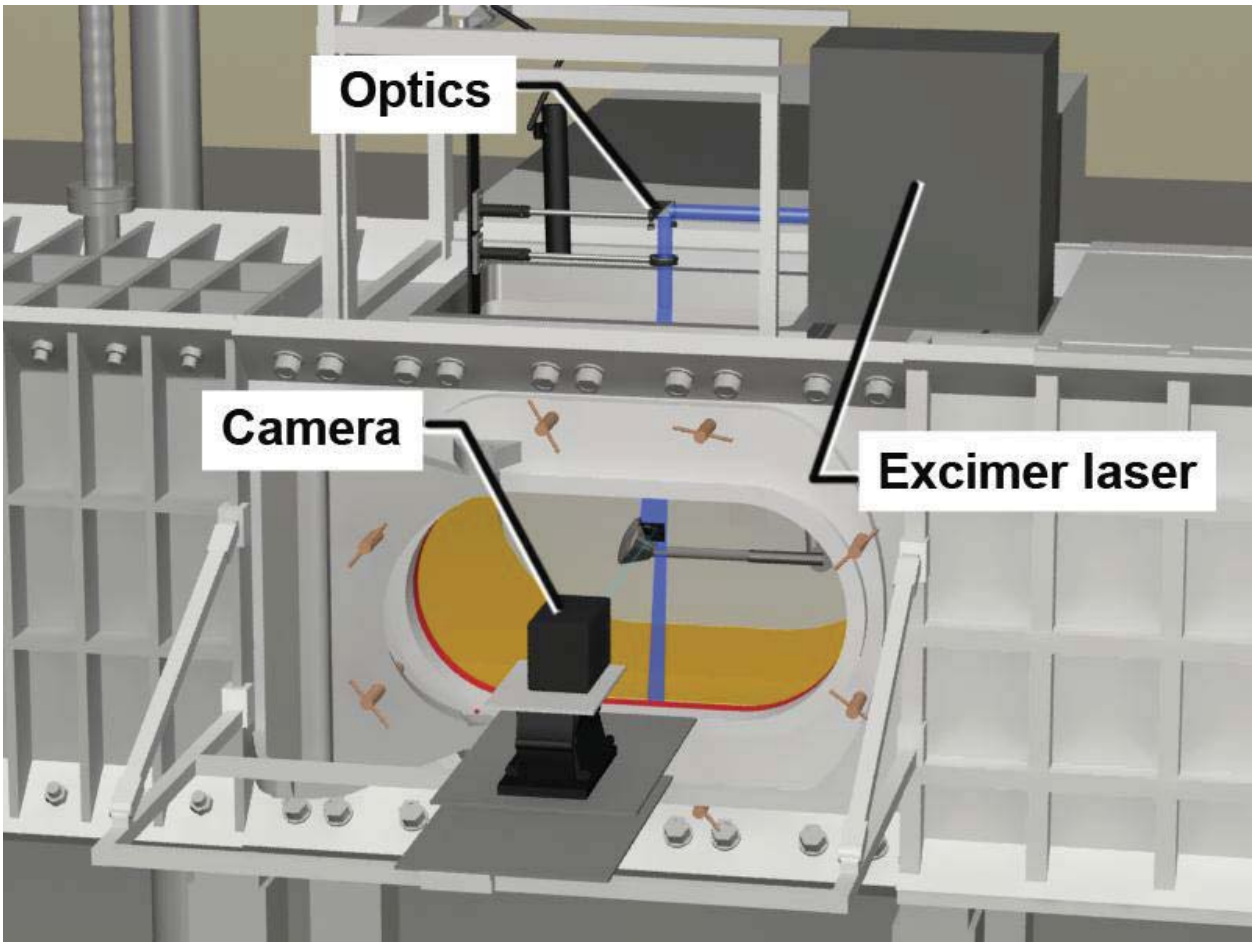

Fig. 1 ViDI rendering of UV iodine LIF velocimetry in the 31M10 wind tunnel.

A. Multipurpose Crew Vehicle Model

Three schematic views of the model are shown in Figure 2. It is an early version of the Crew Exploration Vehicle (CEV) or Orion Spacecraft that is based on the Apollo geometry. Recently, it has been renamed a MultiPurpose Crew Vehicle(MPCV). It is 4 inches in diameter (2% scale). The heat shield radius is 1.2 times the diameter, the corner radius is 0.05 times the diameter, and the back-shell angle is 33 deg. The model is attached to a sting at a 28 deg angle, which was approximately the entry angle of attack of Apollo. Pressure orifices are positioned in the front, top, bottom, and rear of the model. Essentially, this was a model of convenience used to create a shock jump and to evaluate wake and other measurement possibilities. Pressure is measured using ports 1,3,5,7, and 15. Port 15 is 19.1 mm from port 3. All ports have a 1.5 mm diameter orifice. Forebody temperature is measured by a thermocouple(not shown) inside the model and in contact with the forebody near port 7. The model is coincidentally rotated 28 degrees counterclockwise off centerline to prevent laser scatter off model backshell and sting. The sting is at zero pitch.

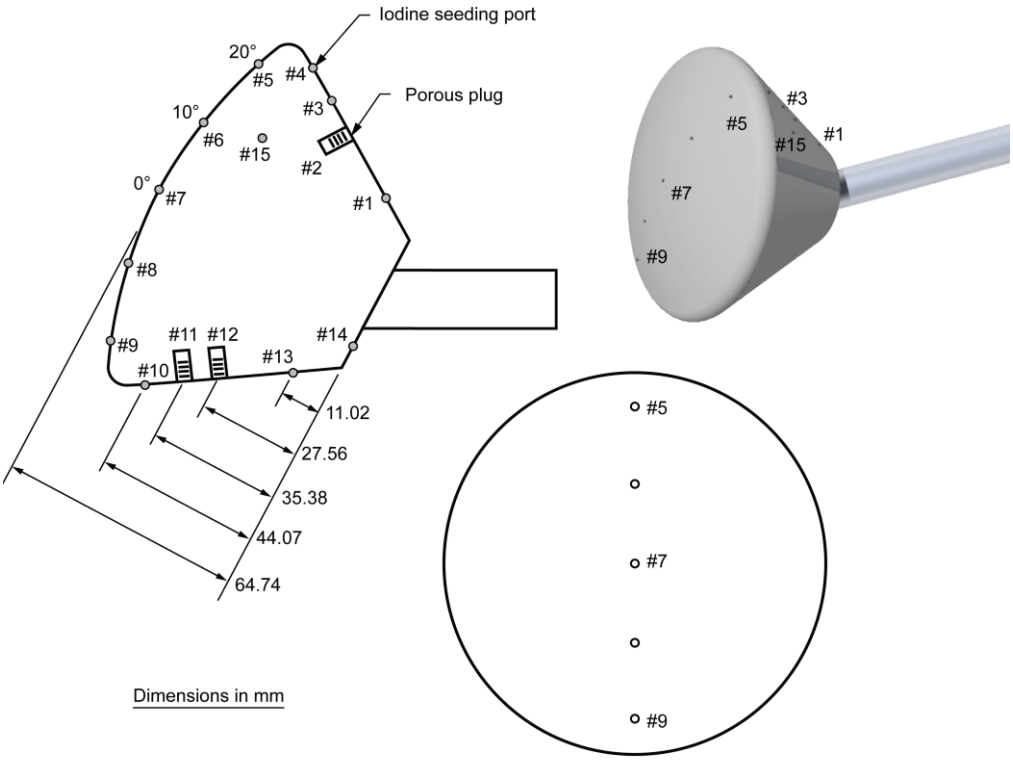

Fig. 2 MPCV– three schematic views

B. Iodine Seeding

I_2 seeding has been described previously [4]. It is summarized here for completeness. I_2 is locally heated in a mixing chamber behind the rear tunnel wall to improve sublimation. The iodine/nitrogen-carrier-gas mixture traverses ~ 1 meter of stainless steel tubing inside the strut and sting. Mixture pressure is 0.138 MPa (20 psi). It exits through a 1.5 mm diameter orifice in the model surface at a rear pressure port. This internal tubing is heated by conduction and convection by the hypersonic flow. The iodine in this tubing equilibrates with the tubing temperature prior to exiting at the rear pressure port. Hence, iodine and carrier gas are subject to no abnormal heating. Overall, a mixture of 0.5% iodine in nitrogen is seeded from port 4. Iodine is a toxic gas with a threshold limit value of 0.1 ppm. Iodine is present in the atmosphere at < 10 ppb. The iodine has fully sublimated prior to expansion in the wake jet. There are no known chemical reactions between the ground electronic state of molecular iodine and air under the temperature and pressure conditions present in a Mach 10 wake generated by electrically-heated hypersonic nitrogen or air flows.

C. Wind Tunnel Velocimetry

For velocity measurements, the laser is operated in broadband mode using a stable resonator. Focused laser energy inside the facility is 2.5 mJ. Emission is imaged

at 90 degrees to the flow with a Nikon 105 mm f/4.5 UV-Nikkor lens(25 mm diameter) focused using 193-nm- scattered light. No interference filter is used. Emission is observed using a gated, double-intensified ITT Model F4577 CCD camera. A ViDI rendering of the MPCV model with sting, iodine jet, and velocity measurement location is shown in Figure 3.

Data is acquired at 30 Hz. Ambient stray light was minimized using a 200 ns intensifier gate and extinguishing the room lights. Laser timing jitter was ± 100 nsec. Starting location is visualized using Rayleigh scattering from atmospheric pressure static air inside the facility. CCD camera gate delay times of 5 and 10 μsec are introduced using a delay generator triggered using the field index pulse. Ten seconds are required to set camera gain. The computer can acquire 371 images (64 Megabytes of memory) during a 12.4 second time interval. Six seconds are required to store the data. This process is typically repeated twice during a single windtunnel run.

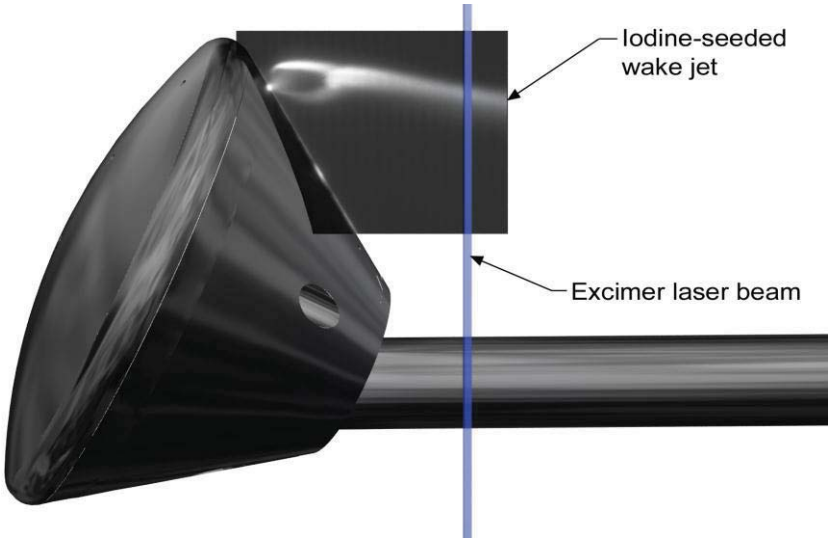

Fig. 3 ViDI rendering of MPCV model, iodine jet, and velocity measurement location.

D. Laboratory Spectrally-Resolved Time-dependent Iodine Emission

Prior to the wind tunnel entry, laboratory experiments were performed to obtain insight into the iodine emission mechanism. The experimental configuration has been described previously[22]. It is similar to the laser configuration shown in Figure 1. A cell with iodine replaces the wind tunnel and a spectrograph replaces the camera. Briefly, the broadband excimer laser is focused into an iodine cell evacuated to ~ 0.1 Torr air. Iodine density is maintained at 1×10^{15} cm^{-3} using an ice-bath cold finger at 273K. Emission 90 degrees to the laser beam propagation direction is collected and filtered using two 4-in.-diam. by 500 mm focal length lenses, i.e., 1:1 imaging. Emission is resolved using an Acton Research Corporation model SP-588 SpectraPro-500i imaging spectrograph/monochromator with 200 μm slit setting and 3600 line diffraction grating blazed at 240 nm. The slit height is 12 mm. Emission is detected with an EMI

Model 9781B photomultiplier tube, digitized, and stored using a 1 GHz digital oscilloscope. Emission is also detected using the intensified gated CCD camera described in section II C.

E. Laboratory Iodine Fluorescence Imaging

Following the successful wind tunnel entry, an experimental setup similar to figure 1 was constructed in the laboratory. A cell with iodine densities equal to those described in section II.D replaced the wind tunnel and a home-built four-inch diameter four-element lens for increased optical collection in addition to the one-inch Nikon lens was used. The lens consists of four 100-mm diameter Suprasil-1 fused silica lenses manufactured by ESCO products with the following shape, focal length, center thickness and lens-to-lens center spacing characteristics in mm (lens 1-biconvex, +150 mm, 23 mm, 30 mm; lens 2-plano-concave, -148 mm, 2.97 mm, 30 mm; lens 3-biconvex, +150 mm, 23 mm, 35 mm; lens 4-plano convex, +250 mm, 30 mm). Focal lengths are specified at 248 nm. A series of 5 apertures with inner diameters of 75, 75, 75, 60, and 32 mm were placed between each successive lens to reduce off-axis rays and improve resolution.

III. Results and Discussion

A. Windtunnel Velocimetry Images

Iodine Tagging Velocimetry(ITV) beginning with at least two photon ArF excitation of molecular I_2 is demonstrated for the first time in Figure 4. This approach monitors $I\ ^2P_{3/2} \rightarrow I\ ^2P^0_{1/2}$ emission at 206 nm in the near wake of a MPCV model.

Figure 4A is the composite of three separate time-averaged images; one showing ITV start position using Rayleigh scattering and two showing ITV time-averaged downstream iodine fluid transit times of 5 and 10 μsec. Images at these transit times are readily achieved by combining the CCD camera gating and variable gain capabilities. Each of the three images in Figure 4A is the average of 371 instantaneous images.

Use of UV I_2 PLIF to identify the start position is hindered by the fact that the edges of the focused laser saturate the Cordes band transitions and broadband molecular emission at t=0 μsec overwhelms atomic emission. The result is a top-hat line image with poorly defined center point. Hence, start position is determined using Rayleigh scattering along the line in Figure 4A. Laser beam was angled slightly to minimize scatter off the model. The laser is positioned 38.2 mm (25.5 jet diameters) downstream of the iodine jet from pressure port #4. Images are cropped to 8.6 mm high by 14.8 mm wide.

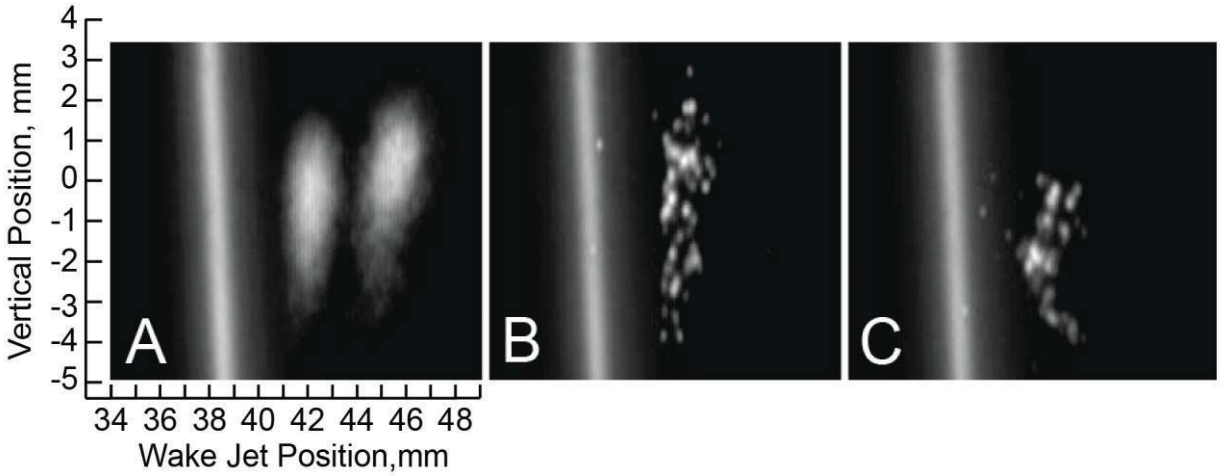

Fig. 4. Iodine tagging velocimetry A) time averaged composite images at 0, 5 and 10 μsec transit times, B,C) instantaneous images at 5 μsec transit times.

In Figure 4A, distances from Rayleigh image to first iodine image(3.774 mm, 68 pixels), second iodine image(7.135 mm, 130 pixels) and distance between iodine images(3.361 mm, 62 pixels) yield velocities at the center of the jet of 750, 710, and 670 m/sec respectively. The mean velocity of 710 m/sec is ~50% of freestream velocity. CCD gain was increased to camera maximum (~ 1000x the Rayleigh gain) to visualize both iodine images. Emission intensity at 10 μsec transit time was multiplied by 3 to produce intensities similar to the 5 μsec transit time for presentation purposes. Time-averaged errors are conservatively estimated using full-width at half maximum (FWHM) of each image at 10%. Results show velocity decreases with increasing distance from the jet.

To verify repeatability, a second set of data at identical transits were acquired during each run. Results are equivalent to those in figure 4. For this proof-of-concept test, data was only acquired at a single stagnation condition of 2.41 MPa (350 psi) and 990K. Fluid conditions at the locations probed in the I_2/N_2 jet in Figure 4 are 300-400K, 0.13 x 10^{17} molecules/ cm^3 N_2 and 0.42 torr air [4]. Figure 1 shows that the relative positions of the laser beam, iodine jet, and CCD camera field-of-view are fixed since all are mounted to the facility. Therefore, images are independent of any bulk facility motion due to heating effects during a run.

Figure 4B is one of the 371 instantaneous velocity images averaged to form Figure 4A at 5 μsec transit time. Similar unique patterns are observed in each instantaneous image. These patterns vary shot-to-shot. Causes of this spatially-localized nonuniform emission are discussed in section IV.C below.

Figure 4C is one of the instantaneous albeit unusual images averaged to form Figure 4A. It is presented to show the shot-to-shot extent of the vertical spatial motion of the shear layer. It is spatially deformed relative to Figure 4A and 4B. It is included to show the capability of this instrumentation for visualizing flow unsteadiness.

In figure 4, no light source inside the wind tunnel was available at 206 nm. The CCD camera was focused using Rayleigh scattering from 1 atmosphere of air at 193 nm. Chromatic aberration in the compound lens is responsible for slight image blurring for the emission observed at 206 nm. Using a single-intensified CCD camera with proper focusing, each point of emission will correspond to ~2 pixels.

Due to 31M10 facility runtime constraints, no resolved emission studies were performed. However, any possible emission above ~ 250 nm in figure 4 would be out-of-focus due to chromatic aberration of the compound imaging lens. Data in section IV.A and IV.B indicate only long-lived emission at 206 nm is present. Based on all these facts, Figure 4 results are attributed to I ($^2P_{3/2}$) → I ($^2P^0_{1/2}$) emission at 206 nm.

B. Wake Jet Velocity Spatial Profile

Visual inspection of the rotated downstream images in Figure 4A indicates a considerable velocity gradient at this spatial location. Velocities normal to the exciting laser beam at 44 points along a 5.5 mm line for the 10 μsec transit time data in Figure 4A are shown in Figure 5A. The transverse velocity component is not measured. Velocities vary from 630 to 820 m/sec(30%) across the 5.5 mm iodine jet and increase toward the shear layer. Velocities show only minor variation from -2 to -3.5 mm. As described, errors are estimated at conservatively 10%. Profile in Figure 5A can be overlaid with textbook shear layer profile near U_2 shown in Figure 5B. Iodine does not penetrate sufficiently into the shear layer for velocities to flatten as shown in Figure 5B. Hence, extrapolation of Figure 5A results suggests gas velocity within and beyond the shear layer are > 820 m/sec or > 59% of freestream velocity. Since the wake jet gas temperature is ~300K [4], jet Mach number varies from ~ 1.9 to ~ 2.4 across figure 5A.

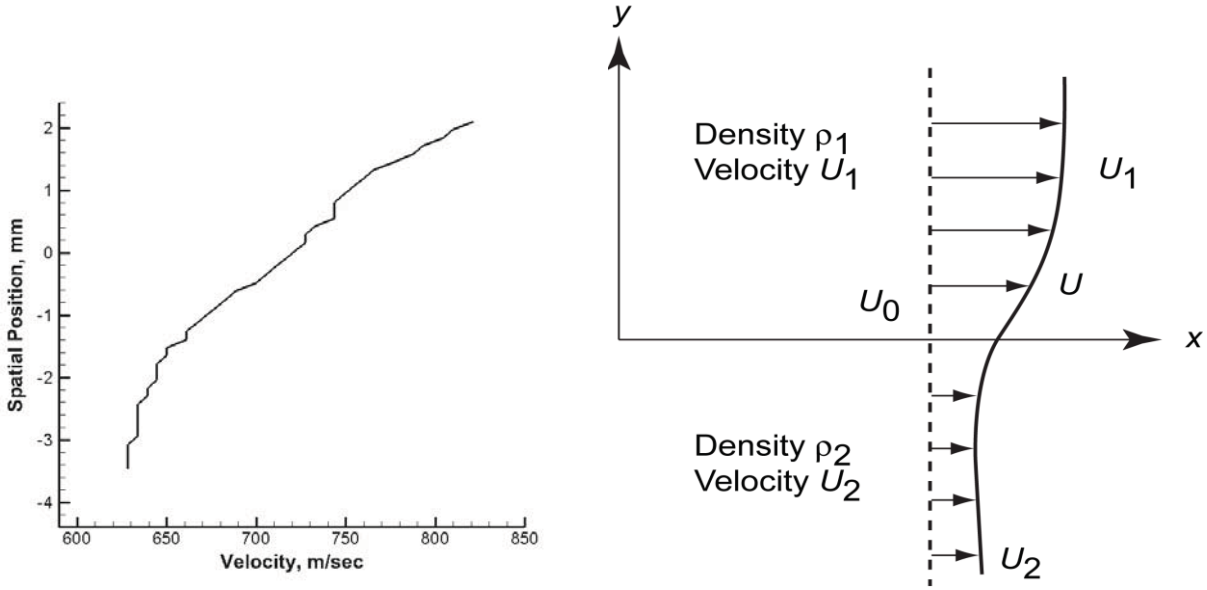

Fig. 5. Spatial velocity profile A) Wake jet and B) textbook shear-layer

C. NO PLIF Velocimetry Comparison

There have been no velocity measurements under identical experimental conditions and at the locations probed in Figure 4. However, NO PLIF has been used to visualize and measure jet velocities within a few jet diameters under somewhat similar conditions. NO PLIF [14] used a 5-inch diameter Orion CEV model, yaw reaction control system(RCS) jet, metal forebody and plastic aftbody, and seeding from port 3 at 18 degree angle of attack. The yaw RCS jet nozzle throat diameter was 0.7 mm (0.0275 in.) with an exit-to-throat area ratio of 22.5. Prenozzle chamber pressures were 0.31 and 0.91 MPa (45 and 132 psi). Stagnation pressure was 2.41 MPa(350 psi).

NO PLIF measurements showed jet centerline velocities varied from 600-800 m/sec essentially independent of jet pressure 0.31 and 0.91 MPa (45 and 132 psi jets) and downstream distances (1 to 15 mm) from jet exit. These measured, averaged velocities are similar in magnitude to those observed downstream in Figure 5A. CFD calculations [14B, 24] showed similar results and spatial trends to NO PLIF results. It was observed that differences between experiment and computation increased with increasing downstream distance and near the edges of the jets. Johansen et al. [24] performed numerical predictions of a Mars Science Laboratory aeroshell reaction control jet interacting with a Mach 10 hypersonic flow. Wake shear layer velocities were 650-800 m/sec, also in good agreement with figure 5A results.

Iodine ATV errors are conservatively 10% (20 psi chamber pressure) while NO PLIF MTV errors at the furthest downstream distances probed (8 mm at 45 psi and 15 mm at 132 psi chamber pressure) were at least 30%. The natural NO A state lifetime is 220 nsec. Quenching in this flow field reduces this to about ~130 ns. NO emission was visualized after 500 ns (~4 lifetimes) yielding typically 6-8 pixels of fluid displacement. Iodine emission is observed for 5-10 μsec or ~ 10-20x the NO A state emission yielding 68 or 130 pixels of fluid displacement. The result for constant velocity flows is lower velocity measurement uncertainty errors are realized with the I_2 LIF measurement. Due to the different NO LIF measurement conditions, data uncertainties, and measurements at different spatial locations, it is concluded that NO LIF velocity measurements cannot be compared directly with the iodine PLIF results in Figures 4 and 5A. However, ignoring their differences, they are to first order in agreement within 20-30%. This suggests the wake flow field created using P_o = 350 psi and similar model shapes is only weakly influenced by the differences in these experiments.

IV. Iodine Tagging Velocimetry Mechanism

The mechanism behind iodine tagging velocimetry (ITV) is not fully understood. The term ITV is used to include the possibilities of both molecular and atomic tagged states. It is known that molecular iodine is seeded in the wake, excited by an ArF excimer laser, and atomic iodine emission at 206 nm is observed. This section discusses possible mechanisms and presents the most likely mechanism based on literature information and experimental results in the present manuscript. Since emission is observed from atomic iodine and emission in the iodine-seeded wake jet is

observed downstream only where the focused laser overlaps the iodine-seeded jet, emission is attributed to iodine and not air constituents.

Single photon absorption in I_2 using an ArF excimer laser occurs near 193 nm via the Cordes bands ($D^1\sum^+_u \leftarrow X\ 1\sum^+_g$) with a lifetime of 15.5 ns [35], 1 x 10^{-17} cm^2 cross section[36], and fluorescence quantum yield ~1 [37]. Later research produced a more exact cross section of 2 x 10^{-17} cm^2 [38]. There are 18 predicted ion-pair electronic states arising from I^- (^1S) + I^+ (^3P,^1D) accessible with ArF laser excitation [39]. All should have similar potential curves, large dissociation energies, small vibrational and rotational energy-level spacing, large internuclear separations, and ~ 10 ns lifetimes similar to $D^1\sum^+_u$. The D' $^3\pi_{2g}$ state lifetime produced by D to D' collisional energy transfer is 6.7 ns [40].

The iodine emission spanning 190-350 nm at < 1 Torr pressure from single-photon absorption near 193 nm is well known[20]. Lifetimes of these states are < 15 ns. None of these molecular states can account for the velocimetry results where emission lasts > 10 μsec. Hence single photon absorption cannot account for the observed long-lived emission.

A. Spectrally-resolved Iodine Emission Spectrum

To obtain insight into the mechanism responsible for long-lived iodine emission, laboratory experiments were performed in an iodine cell using a laser configuration similar to Figure 1 and described in section II. Iodine is excited with a broadband ArF excimer laser near 193 nm. Time-resolved spectra are detected behind a 0.5 m spectrograph using a gated intensified CCD camera. An emission spectrum beginning at a time delay of 0.3 μsec following the laser pulse is presented in Figure 6. Gate width is 0.5 μsec and 50 lines on the detector were summed. Fluorescence is observed at 206.16 nm. Similar scans were performed from 220-400 nm. No additional fluorescence was detected.

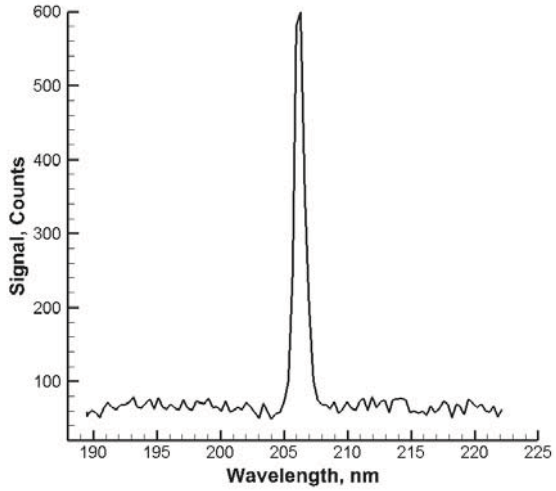

Fig. 6 Iodine emission spectra delayed 0.3 μsec from laser pulse

B. 206 nm Time-Dependent Iodine Emission

To obtain insight into the iodine emission mechanism and expand on the results in section IV.A, the CCD camera was replaced with a phototube. Tuning the laboratory spectrometer to 206.16 nm to observe fluorescence from I ($^2P_{3/2}$) → I ($^2P^0_{1/2}$), the time-dependent emission profile in figure 7A is observed.

The first and largest peak in Figure 7A near t = 90 ns is saturated and composed primarily of I_2 ($D^1\sum^+_u \rightarrow X\ 1\sum^+_g$) emission. D → X emission decays in ~ 26 ns after which I ($^2P_{3/2}$) → I ($^2P^0_{1/2}$) emission at 206 nm grows to create the second weaker peak with an 84 ns induction time measured from the pulse start at 62 ns. Emission continues to decay for 1000 nsec. This time constraint is dictated mainly by a digitizer with 8-bit dynamic range. Figure 7B shows a plot of the natural log of the signal (Ln) in Figure 7A vs time. Using a linear-least-squares straight-line fit spanning 200-500 ns, a first –order decay process was observed with a lifetime of 196 ns.

Initial lifetime measurements for a variety of atomic iodine transitions were first reported by Lawrence[41]. Emission from 206 nm and 178 nm originate from the same excited state ie. I ($^2P_{3/2}$). Lawrence *incorrectly* identified this state as I ($^4P_{3/2}$)*. The natural lifetime of excited atomic iodine states with emission spanning 150-206 nm is typically 3 to 60 ns [41]. Emission ratio of the 178 and 206 nm lines is 92:1 [41]. Emission lifetime of I ($^2P_{3/2}$) at 206 nm is 3.6 ns[41] using the formula Tau(I ($^2P_{3/2}$) = 1/ ∑ (A(178 nm) + A(206 nm)).

* J. Tellinghuisen, personal communication, 2012

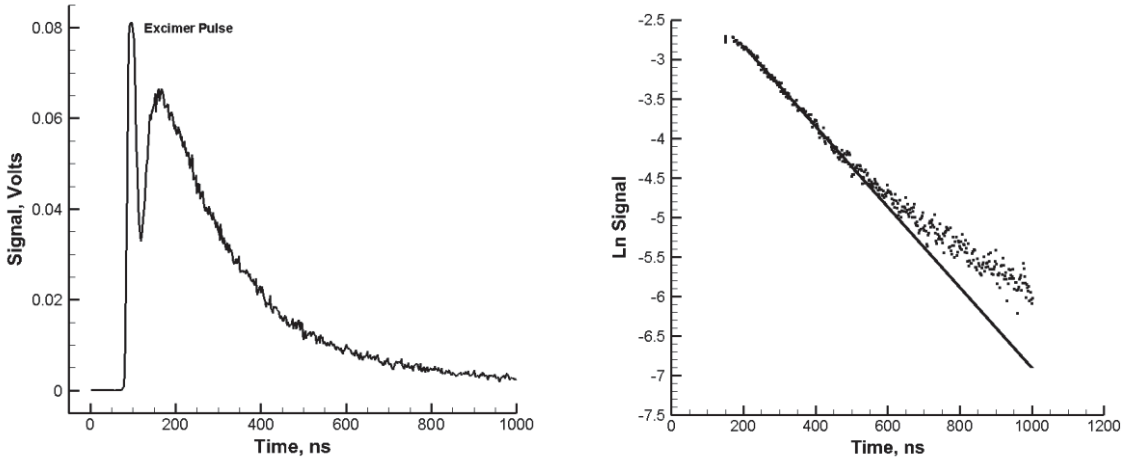

Fig. 7 A) Atomic iodine emission at 206.16 nm versus time. B) Ln signal from Fig. 7A vs time and linear fit

Here, A designates the Einstein A-coefficient for spontaneous emission Under conditions where oxygen and its deleterious absorption effects can be excluded from the emission path, signal levels in Figure 4 can be increased by ~100x by monitoring emission at 178 nm.

Based on the known atomic and molecular iodine emission lifetimes discussed, the long-lived emission observed in Figures 4,6, and 7 cannot be attributed to radiative properties of iodine atoms. Since the bond dissociation energy for I_2 is 148.8 kJ/mole [42], energy requirements for 206 nm emission dictate at least a two photon absorption process. In addition, the long lifetime in Figures 4, 6 and 7 dictate a process capable of storing energy for at least 1 μsec(30 μsec based on results in section IV.C below).

C. Iodine Fluorescence Imaging in a Static Gas

Following the successful wind tunnel velocimetry results, an experimental setup similar to figure 1 and described in the experimental section was assembled in the laboratory. An iodine cell replaced the wind tunnel. Instantaneous images (200 ns shutter) at room temperature in non-flowing iodine at a density of 1 x 10^{15} cm^{-3} and 298K are shown in Figure 8A-D. Images are cropped to show only 7 mm (20%) of the imaged line. Single-shot images using the 25 mm diameter aperture Nikkor lens and CCD camera delay times from the laser pulse of 0.2, 2, 5, and 10 μsec are shown in figures 8A-D. Averaged images(371 single shots) using the 100 mm diameter aperture home-built lens and CCD camera delay times of 20 and 30 μsec are shown in figures 8E-F. Signal levels between Figures 8A and 8F decrease by ~ 6400x.

Instantaneous images show a transition from spatially-uniform emission (Figure 8A) at short delay times to spatially-localized nonuniform emission(Figure 8C, 8D) at longer delay times. Based on the results and spectroscopic discussion in section IV.A and IV.B, emission in Figure 8 is attributed to I ($^2P_{3/2}$) → I ($^2P^0_{1/2}$) emission at 206 nm. The spatially-localized nonuniform emission at long delay times is a result of low photon statistics at long delay times (< 10 photoelectrons per pixel), detector gain at the maximum setting, and a nonadjustable mismatch between the DC levels of the CCD camera and digitizer producing a negative baseline. All emission is spread to ~4 pixels by the double-intensified CCD camera.

Averaged images show the improvement in delay times using the 100 mm diameter lens. Note that S/N is ~ 6 and ~ 3 in Figures 8E and 8F respectively.

D. Iodine Tagging Velocimetry Excitation and Emission Mechanism

The ionization energy of I_2 is 9.3074 electron volts(eV) [43]. A two photon absorption process using 193 nm radiation has 12.83 eV. This will ionize I_2. Data on multiphoton ionization of I_2 is sparse. Martin et al. [44] provided evidence for a strong resonant two photon transition in iodine using an ArF excimer near 193 nm along with significant amounts of ions(~ 10^{12} cm^{-3}) and therefore electrons. The second photon cross section, estimated at ~ 10^{-16} cm^2, is exceptionally large. Since this cross section is 10x the D ← X cross section, the second absorption process is saturated and this two photon process is *linear* with laser energy. They noted that this state lies well above the

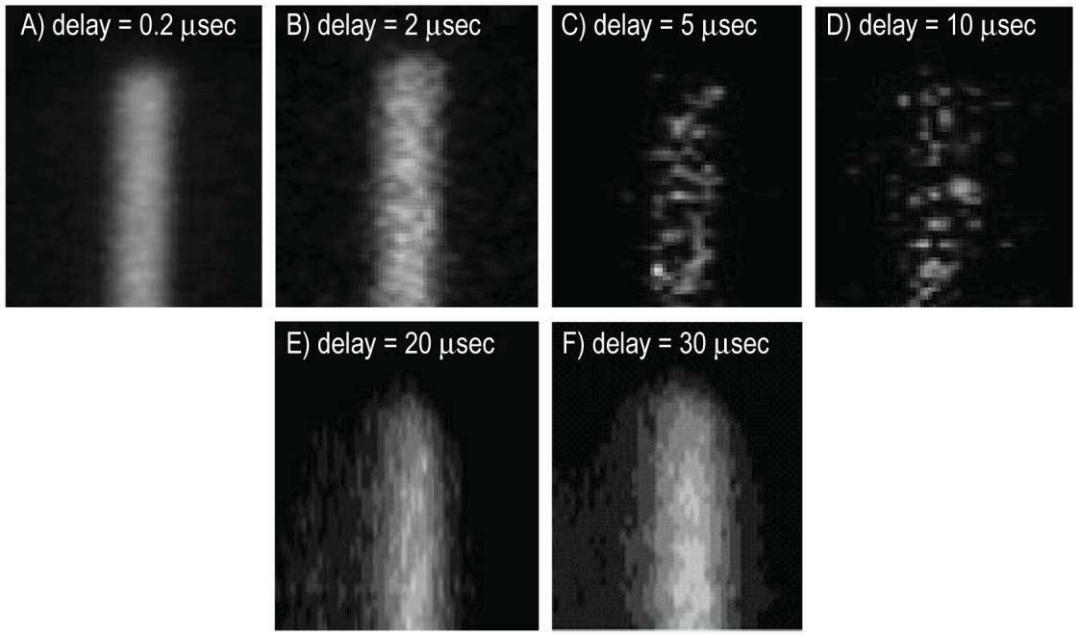

Fig. 8. Laboratory iodine fluorescence time-delayed images A-D) single-shot images using 25 mm aperture Nikon lens, E-F) average images using 100 mm aperture lens.

atomic ionization threshold and the two-photon process is resonant with the $^2\sum^+_g$ state of I_2^+. Two photon excitation of I_2 can produce electrons with up to 3.5 eV of translational energy. Hewitt et al. [45] used these "hot" electrons to excite V" = 2 in CO_2 and V" = 1 in CO.

This paragraph is taken from Hewitt et al[45]. There are five known I_2^+ states that lie at or below the energy of 2 photons at 193 nm [46]. These include $X\ ^2\Pi_{3/2g}$ (9.34 eV) , $X\ ^2\Pi_{1/2g}$ (9.98 eV), $A\ ^2\Pi_{3/2u}$ (11.0 eV), $A\ ^2\Pi_{1/2u}$ (11.81 eV), and $B\ ^2\sum_g^+$ (12.95 eV). The X states are relatively stable with a lifetime of ~ 14 μsec [47]. Some of the ions in the A states dissociate, and the B state is completely dissociated into I^+ ($^3P_2$) and I ($^2P_{3/2}$) ground state[47]. There are four Z-states in I_2^+ which lie between the 2 and 3 photon energies of 193 nm photons. In the dissociation limit, they produce I^+ (^3P) cations and I (^2P) atoms with 3.9 eV of translational energy[46].

O'keefe et al. [30] showed it is possible to form high-n Rydberg atoms(I*) from the neutral dissociation of super excited states of I_2 following two photon absorption at 193 nm. Molecular Rydberg states are considered to be a super excited state(SES) when the neutral excited state has internal energy greater than the lowest ionization threshold of the molecule. Upon excitation the SES will predissociate into a ground state atom I($^2P^0_{3/2}$), and a high-n Rydberg iodine atom. They showed that high-n Rydberg atoms(I*) are formed by predissociation of the optically excited molecular Rydberg states $I_2^*[R(B^2\sum^+_g)]$ which converge on the $I_2^+[R(B^2\sum^+_g)]$ state of the ion. For the $I^*(R^3P_2)$ fragment of this molecular ion, the average Rydberg lifetime is 325 ± 25 μsec.

Recent measurements have shown that wake pressures in this experiment are 0.42 Torr [4]. Mean free path is ~0.2 mm. Therefore, this state would be quenched in a few collisions corresponding to < 60 ns. This is in reasonable agreement with the induction time in Figure 7A. However, assuming 10 ns atomic lifetimes and assuming iodine forms in an electronic state which eventually cascades to the $I\ ^2P_{3/2}$ state from which 206 nm is observed, known emission lifetimes cannot account for the 10 μsec lifetime in Figure 4. Therefore, under the conditions present in this Mach 10 wake, long-lived high-n Rydberg states are not responsible for Figure 4 emission.

The next paragraphs consider the possibility of radiative emission from electronically excited iodine trapped in a cluster. Using a free jet expansion similar to the present setup, ArF excimer irradiation of I_2/Ar_n clusters produced I_2 in the D' state [48]. For I_2 in a cluster, many internal energy modes exist for internal energy conversion. Therefore, it is not surprising that emission lifetimes follow the laser pulse width of typically 20 ns[48]. I_2 in the D' state was stabilized by the argon cluster and shown to persist for 7 μsec. However, a second laser was required to generate fluorescence from this species.

Figure 4 results are observed in a N_2 jet. I_2/N_2 clusters are difficult to produce and generally require freestream temperatures < 150K. In a free jet expansion with rotational I_2 temperature of 10K [49], fluorescence from I_2 rare-gas clusters of argon, krypton, and xenon has been observed[49]. No clustering or fluorescence was observed with I_2 mixed with nitrogen, helium or neon. Johnson and Levy [50] produced I_2/N_2 clusters by expanding a mixture of 1% N_2, 99% helium, with iodine saturated at its room temperature vapor pressure at a total pressure of 1000 psi through a 25 μm supersonic nozzle. Downstream pressure was ~ 0.1 Torr.

Marshall et al. [51] produced I_2/N_2 clusters by expansion of a mixture at 300K through a Mach 5 nozzle to ~60K in a chemical oxygen-iodine laser (COIL) laser experiment. This process removed free iodine and thereby reduced lasing efficiency. A cluster-buster wire mesh created a bow shock which raised the temperature to > 160K and destroyed the I_2/N_2 clusters.

Since I_2 seeding in the present study is identical to a previous study[4], it is concluded that I_2 density in the wake jet of figure 4 is 2.5×10^{14} molecules/cm^3 or ~0.5% of jet air density. Wake jet temperatures at the locations probed in Figure 4 are ~ 300-400K [4]. At these temperatures, I_2/N_2 clusters cannot exist. I_2/N_2 stagnation pressures were 20 psi; a negligible fraction of reference 50. Excitation of I_2/Ar_n clusters using an ArF excimer laser produced emission lifetimes of ~ 10 ns. This is 1000x less than figure 4 results. It is consistent with the fact that clusters can be thought of as a liquid. Hence, they have a large number of energy modes available for internal energy conversion. Based on these facts, the present study finds no evidence to support the existence of clusters at these wake temperatures. Even if they exist, there is no evidence to support the concept of iodine emission within a homogeneous I_2 cluster or a heterogeneous I_2/N_2 cluster or any iodine chemical reaction within a cluster producing emission observed in Figure 4 on a time scale spanning 10 μsec.

As discussed throughout this manuscript, I_2^+, I^+, I^-, "hot" electrons and thermal electrons are being produced by two or more photon absorption in iodine. The literature contains iodine energy level diagrams to aid the reader[37,52]. The possibility of a long-

lived energy storage mechanism involving high-n Rydberg states has been discounted due to the pressures in this wake. Since no known radiative properties of neutral or ionic iodine atoms or molecules can produce the observed long-lived emission, attention is given to chemical processes. They must be capable of storing energy for >10 μsec and releasing it via a mechanism which produces 206 nm emission. Possibilities based on exothermic thermochemical considerations are given in reactions 1-3. I refers to a ground electronic state iodine atom and I** refers to a highly electronically excited iodine atom. For both I and I**, the energy levels are not specified. M represents a buffer gas which can remove excess energy by collisions. Reactions 1 and 3 represent electron-ion recombination. Reaction 2 represents ion-ion neutralization.

$$I_2^+ + e^- \rightarrow I\ ^2P_{3/2} + I \qquad 1$$

$$I^+ + I^- + M \rightarrow I\ ^2P_{3/2} + I + M \qquad 2$$

$$I^+ + e^- \rightarrow I^{**} + M \rightarrow I\ ^2P_{3/2} + M \qquad 3$$

In inductively-excited radio-frequency discharges at pressures of 0.5-5 Torr, these reactions were postulated[52] as possible mechanisms for producing long-lived emission at 206 nm and 804 nm ($^4P^0_{3/2} \rightarrow {}^4P_{5/2}$) which was observed for ~ 600 μsec. Barnes and Kushnera[52] attributed this long-lived emission to reaction 2.

The large exothermicity of reaction 2 and particularly reaction 3 requires collisions from a buffer gas to remove excess energy in the collision complex and allow the reaction to proceed. At wake pressures of ~ 0.42 Torr in the present study, the probability of collisional stabilization is negligible. Therefore, kinetic considerations tend to discount reactions 2 and 3. In contrast to reactions 2 and 3, I_2^+ is a molecule. It has more internal energy modes available for energy transfer and can release energy by dissociation following the recombination. No collisions are required to stabilize the collision complex.

Hemmati and Collins[37] attributed 206 nm emission observed following ArF two-photon excitation to reaction 1. Additional support came from addition of 0.5 Torr SF_6 which effectively scavenged the thermal electrons and quenched the 206 nm emission.

Literature evidence and discussions in the present study suggest that 206 nm emission results from reaction 1. If thermal electrons are required for reaction 1 to proceed, this may explain the induction time observed in Figure 7A.

For the present proof-of-concept test, the primary interest is demonstrating viability of the diagnostic in a Mach 10 wake. Results in the present study suggest that Figures 4 and 8 are imaging the kinetics of an ion-ion or electron-ion reaction. This reaction provides a long-lived chemical storage mechanism capable of releasing detectable energy on a time scale > 10 μsec. It is hoped the present study will stimulate further research to determine which of these reactions is responsible for ITV results reported in the present manuscript and further elucidate any potential intermediate states in this complex spectroscopic process. It is noted that this two or more photon absorption process is excited using only 2.5 mJ, a high divergence (3 mrad vertical x1 mrad horizontal) unpolarized broadband excimer laser, and 600 mm focal length lens.

Following emission at 206 nm, iodine atoms are deposited in their first excited electronic state I ($^2P^0_{1/2}$). This is a metastable state with 0.1 sec lifetime [25]. Potentially, the I ($^2P^0_{1/2}$) → I ($^2P^0_{3/2}$) transition at 1.315 μm could be monitored to further increase transit time. However, no intensified camera with a gateable infrared photocathode and sufficient quantum efficiency currently exists to take advantage of this process. The reaction between ground-state atomic iodine and oxygen is endothermic and does not occur. Using an I-atom concentration of 2 x 10^{13} molecules/cm^3, the recombination reaction of atomic iodine with itself to form I_2 is negligible in 1 Torr air [53]. Therefore, addition of a probe laser to excite $^2P_{3/2}$ ← $^2P^0_{1/2}$ at 206 nm, I ($^2P^0_{1/2}$) ← I ($^2P^0_{3/2}$) transition at 1.315 um, or I $^2P_{3/2}$ ← $^2P^0_{3/2}$ at 178 nm could further increase transit time at the expense of experimental complexity.

V. Conclusion

The first demonstration of time-of-flight based Iodine Tagging Velocimetry(ITV) is presented. Experiments were performed along a 5.5 mm line in a 0.5% iodine/nitrogen jet in the hypersonic near wake of a capsule entry vehicle model in the NASA-Langley 31-inch Mach 10 air wind tunnel at 350 psi stagnation pressure and 990K stagnation temperature. The original intent of this study was to determine if high-n Rydberg atoms of iodine formed by resonant two-photon 193 nm excitation of molecular iodine could be used for time-of-flight velocimetry. Unfortunately, at the higher than expected wake pressure of 0.42 Torr, collisions quench the high-n Rydberg atoms in < 60 ns. This approach may still be viable at significantly lower pressures. However, a study of this approach has lead serendipitously to the discovery of an alternate iodine-based energy-storage mechanism allowing hypersonic wake velocimetry.

Results suggest I_2 absorbs at least 2 photons to produce I_2^+, I^+, I^- and electrons. I^+ and I^- neutralization and/or the recombination of I_2+ and electrons release this energy over at least 10 μsec as the tagged region is displaced downstream. This process produces I ($^2P_{3/2}$) whose emission is monitored at 206 nm. Extrapolation of results combined with the increased optical collection of a 4" lens developed after the wind tunnel experiments suggests wind tunnel fluid displacement times > 10 μsec can be observed.

The result is a velocity diagnostic well suited for spatially-resolved velocimetry measurements to study the fundamental flow physics of cold-flow hypersonic near and far wakes. This velocimetry method has the added advantage of simplicity through use of a single laser and camera. Additional research is required to identify the reaction mechanism, to understand all the subtleties of this process, and to determine if there are other emission pathways which can be used for velocimetry.

This approach avoids typical toxicity and corrosion problems of iodine using local seeding from a single model pressure port with trace quantities (<2.5 x 10^{14} cm^{-3}) of iodine. Iodine is chemically nonreactive, persists in the flow, and follows streamlines.

References

[1] Boutier, A. (ed.) *New Trends in Instrumentation for Hypersonic Research,* Kluwer, Dordrecht, The Netherlands, 1993.

[2] Bonnet, J. P., Gresillon, D., and Taran, J. P., "Non-Intrusive Measurements for High-Speed, Supersonic, and Hypersonic Flows," *Annual Review of Fluid Mechanics*, Vol. 30, 1998, pp. 231–273.

[3] Estruch, D., Lawson, N. J., and Garry, K. P., "Application of Optical Measurement Techniques to Supersonic and Hypersonic Aerospace Flows," *Journal of Aerospace Engineering*, Vol. 22, No. 4, 2009, pp. 383–395.

[4] Balla, R. J. and Everhart, J. L., "Air Density Measurements in a Mach 10 Wake using Iodine Cordes Bands", *AIAA Journal*, Vol. 50, No.6, 2012, pp. 1388-1397.

[5] Zimmermann, M. and Miles, R. B., "Hypersonic-helium-flow-field measurements with the resonant Doppler velocimeter", *Applied Physics Letters*, Vol. 37, 1980, pp. 885–887.

[6] Exton, R.J., Hillard, M. E., "Raman Doppler Velocimetry: a unified approach for measuring molecular flow velocity, temperature and pressure", *Applied Optics*, Vol. 25, 1986, pp. 14-21.

[7] Miles, R. B., Grinstead, J., Kohl, R. H., and Diskin, G., "The RELIEF flow tagging technique and its application in engine testing facilities and for helium–air mixing studies", *Measurement Science and Technology,* Vol. 11, 2000, pp. 1272–1281.

[8] Miles, R. B. and Lempert, W. R., "Quantitative Flow Visualization in Unseeded Flows", Annual Review of Fluid Mechanics, Vol. 29, 1997, pp. 285–326.

[9] Koochesfahani, M. M., and Nocera, D. G., "Molecular Tagging Velocimetry," Handbook of Experimental Fluid Dynamics, edited by J. Foss, C. Tropea, and A. Yarin, Springer–Verlag, Berlin, 2007, Chap. 5.4.

[10] Dam, N., Klein-Douwel, R. J. H., Sijtsema, N. M., and ter Meulen, J. J., "Nitric Oxide Flow Tagging in Unseeded Air," *Optics Letters*, Vol. 26, No. 1, 2001, pp. 36–38.

[11] Laurendeau, N., M., "Temperature Measurements by Light Scattering Methods, *Progress Energy Combustion Science,* Vol. 14,1998, pp. 147-170.

[12] Danehy, P. M., O'Byrne, S., Houwing, A.F.P., Fox, J.S., Smith, D.R., "Flow-tagging velocimetry for hypersonic flows using fluorescence of nitric oxide," *AIAA Journal*, Vol. 41, No. 2, 2003, pp. 263-271.

[13] Hruschka, R., O'Byrne, S., and Kleine, H., "Two-component Doppler-shift fluorescence velocimetry applied to a generic planetary entry probe model ", *Experiments in Fluids*, Vol. 48, No. 6, 2010, pp. 1109-1120.

[14] A) Bathel, B.F., Danehy, P. M., Inman, J. A., Jones, S. B., Ivey, C. B., and Goyne, C. P. "Velocity Profile Measurements in Hypersonic Flows Using Sequentially Imaged Fluorescence-Based Molecular Tagging", *AIAA Journal*, Vol. 49, No. 9, 2011, pp. 1883-1896.
B) Ivey, C. B., Danehy, P. M., Bathel, B. F., Dyakonov, A. A., Inman, J. A., and Jones, S. B.," Comparison of PLIF and CFD Results for the Orion CEV RCS Jets", AIAA 2011-713.

[15] Hiller, B., and Hanson, R. K., "Properties of the iodine molecule relevant to laser-induced fluorescence experiments in gas flows", *Experiments in Fluids*, Vol. 10, 1990, pp.1–11.

[16] Fletcher, D. G., and McDaniel, J. C., "Laser-Induced Iodine Fluorescence Technique for Quantitative Measurement in a Nonreacting Supersonic Combustor", *AIAA Journal*, Vol. 27, No. 5, 1989, pp. 575-580.

[17] Hiller, B., and Hanson, R. K., "Simultaneous Planar Measurements of Velocity and Pressure Fields in Gas Flows Using Laser-Induced Fluorescence," *Applied Optics*, Vol. 27, No. 1, 1988, pp. 33-48.

[18] Cecil, E. and McDaniel, J. C., "Planar Velocity and Temperature Measurements in Rarefied Hypersonic Flow Using Iodine LIF," AIAA-2005-4695.

[19] McDaniel, J. C., personal communication, taken from Nicholson, L., MS thesis, Department of Mechanical and Aerospace Engineering, University of Virginia, 1985.

[20] Exton, R. J., and Balla, R. J., "ArF Laser Excitation, Collisional Transfer, and Quench-free Fluorescence in I_2 / foreign gas mixtures", *Journal of Quantitative Spectroscopy and Radiative Transfer*, Vol. 86, 2004, pp. 267-283.

[21] Exton, R. J., Balla, R. J., Shirinzadeh, B., Hillard, M. E., and Brauckmann, G., "Flow Visualization using Fluorescence from Locally Seeded I_2 Excited by an ArF Excimer Laser", *Experiments in Fluids*, Vol. 26, 1999, pp. 335-339.

[22] Balla, R. J. and Exton, R. J., "Density Measurements in Air by Optically Exciting the Cordes Bands of I_2", Measurement Science and Technology, Vol. 11, 2000, pp. 459-466.

[23] Balla R. J. and Exton, R. J., "Thermometry in Air by Optically Exciting the I_2 Cordes Bands", Measurement Science and Technology, Vol. 11, 2000, pp. 1319-1327.

[24] Johansen, C. T., Nowak, L., Bathel, B., Ashcroft, S. W., Danehy, P. M., "Comparison of MSL RCS Jet Computations with Flow Visualization and Velocimetry", AIAA 2012-0594.

[25] Okabe H, *Photochemistry of Small Molecules*, Wiley, New York. 1978. Table A-2. p. 363-372.

[26] Liebeskind, J. G., Hanson, R. K.., and Cappelli, M. A., "Laser-induced fluorescence diagnostic for temperature and velocity measurements in a hydrogen arcjet plume", *Applied Optics*, Vol. 32, No. 30, 1993, pp.6117- 6217.

[27] Marinelli, W. J., Kessler, W. J., Allen, M. G., Arepalli, S., and Scott, C. D., "Copper atom based measurements of velocity and turbulence in arc jet flows", AIAA-1991-0358.

[28] Barker, P., Bishop, A., Rubinsztein-Dunlop, H., " Supersonic velocimetry in a shock tube using laser enhanced ionization and planar laser induced fluorescence", *Applied Physics B,* Vol. 64, 1997, pp. 369-376.

[29] Turk, G. C. and Omenetto, N., "Optical Detection of Laser-Induced Ionization: A Study of the Time Decay of Strontium Ions in the Air-Acetylene Flame", *Applied Spectroscopy*, Vol. 40, No. 8, 1986, pp. 1085-1092.

[30] O'Keefe, P., Stranges, D., and Houston, P., "Neutral photodissociation of superexcited states of molecular iodine," *Journal Chemical Physics*, Vol. 127, 2007, pp. 144309.

[31] Mills, J. L., Sukenik, C. I., and Balla, R. J., "Hypersonic Wake Diagnostics Using Laser Induced Fluorescence Techniques", AIAA 2011-3459.

[32] Balla, R. J. and Everhart, J. L., "Rayleigh Scattering Density Measurements, Cluster Theory, and Nucleation Calculations at Mach 10", *AIAA Journal*, Vol. 50, No.3,2012, pp.698-707.

[33] Micol, J. R., "Langley Aerothermodynamic Facilities Complex : Enhancements and Testing Capabilities," AIAA Paper 98-0147.

[34] Schwartz, R. J., and McCrea, A. C., "Virtual Diagnostics Interface: Aerospace Experimentation in the Synthetic Environment," MODSIM World 2009 Conference and Expo, Virginia Beach, VA, Pinelli, T. E. (ed.), NASA Langley Research Center CP NASA/CP-2010-216205, Hampton, VA, Oct. 2009, pp. 103–108.

[35] Callear, A. B., Erman, P., and Kurepa, J., "The D state lifetime and the UV laser action of molecular iodine" *Chemical Physics Letters,* Vol. 44, 1976, pp. 599–601.

[36] Myer, J. A., and Samson, J. A. R., “Absorption cross section and photo ionization yield of I_2 between 1050 and 2200 A” *Journal Chemical Physics*, Vol. 52. 1970, pp. 716–18.

[37] Hemmati H. and Collins, G. J., “Laser excited fluorescence of I_2”, *Chemical Physics Letters* , Vol. 75, No. 3, 1980, pp. 488–93.

[38] Tellinghusen, J. and Phillips, L. F., “Kinetics of I_2 following Photolysis at 1930 A: Temperature Dependence of A'-State Quenching”, *Journal Physical Chemistry*, Vol. 90, 1986, pp. 5108-5120.

[39] Mulliken, R. S., “Iodine Revisited”, *Journal Chemical Physics*, Vol. 55, 1971, pp. 288–309.

[40] Sauer M. C. et al, “Fast excited state formation and decay in the pulse radiolysis of gaseous argon–iodine systems”, *Journal Chemical Physics*, Vol. 64, 1976, pp. 4587–91.

[41] Lawrence, G. M., “Resonance Transition Probabilities in Intermediate Coupling for some Neutral non-metals”, *Astrophysics Journal*, Vol. 148,1967, pp. 261-268.

[42] Leroy, R. J. and Bernstein, R.B., “Dissociation Energies and Long-Range Potentials of Diatomic Molecules From Vibrational Spacings: The Halogens”, *Journal Molecular Spectroscopy*, Vol. 37,1971, pp. 109-130.

[43] Cornford, A. B., Frost, D. C., McDowell, C. A., Ragle, J. L., Stenhouse, I. A., “Photoelectron Spectra of the Halogens”, *Journal Chemical Physics*, Vol. 54, No. 6, 1971, pp. 2651-2657.

[44] Martin, M., Fotakis, C., Donovan, R. J., and Shaw, M. J., “Optical Pumping and Collisional Quenching of I_2 $D^1\sum^+_u$ ” *Nuovo Cimento B*, Vol. 63,1981, pp. 300-308.

[45] Hewitt, S. A., Zhu, L., and Flynn, G. W., “Diode laser probing of CO_2 and CO vibrational excitation produced by collisions with high energy electrons from 193 nm laser photolysis of iodine," *Journal Chemical Physics*, Vol. 97, No. 9, 1992, pp. 6396-6409.

[46] Leach, S., “Dissociative Relaxation of I_2^+, Br_2^+ and Cl_2^+ “, *Journal of Physical Chemistry*, Vol. 92, 1988, 5373-5379.

[47] Eland, J. H. D., “Angular Distributions, Energy Disposal, and Branching Studied by Photoelectron-photoion Coincidence Spectroscopy O_2^+, NO^+, ICl^+, IBr^+, and I_2^+”, *Journal Chemical Physics*, Vol. 70 No. 6 , 1979, 2926-2933.

[48] Fei, S., Zheng, X., Heaven, M. C. and Tellinghuisen, J., “Spectroscopy and relaxation dynamics of I_2Ar_n clusters. Geminate recombination and cluster fragmentation”, *Journal Chemical Physics*, Vol. 97, 1992, pp. 6057-6063.

[49] Randall, K.l., and. Donaldson, D.J., “Photophysics and photochemistry of I_2 (D, D') in rare gas clusters”, *Chemical Physics*, Vol. 211, 1996, pp. 377-386.

[50] Johnson, K. E., and Levy, D. H., “The fluorescence excitation and dispersed fluorescence spectra of the van der Waals molecules I_2N_2 and I_2N_2He”, *Journal Chemical Physics* 74,1506-1507(1981).

[51] Marshall, J., Healey, B., Croker, B., Kendrick, K., Yang, T. T., Hsia, Y. C., Dickerson, R. A., and Forman, L., “COIL power extraction enhanced by reducing/eliminating iodine clusters in a high Mach number nitrogen mixing nozzle”, Proceedings of SPIE, Vol. 6101, 2006, pp.61011Z

[52] Barnes, P. N., and Kushnera, M. J., “Ion-ion neutralization of iodine in radio-frequency inductive discharges of Xe and I_2 mixtures”, *Journal Applied Physics,* Vol. 82, No.5, 1997, pp. 2150-2155.

[53] Jenkin, M. E., Cox, R. A., Mellouki, A., Le Bras, G. and Poulet, G., “Kinetics of the Reaction of Iodine Atoms with HO_2 Radicals”, *Journal Physical Chemistry*, Vol. 94, 1990, pp. 2927-2934.

REPORT DOCUMENTATION PAGE

Form Approved
OMB No. 0704-0188

1. REPORT DATE *(DD-MM-YYYY)*	2. REPORT TYPE	3. DATES COVERED *(From - To)*
01- 07 - 2013	Technical Memorandum	2009 - 2013

4. TITLE AND SUBTITLE

Iodine Tagging Velocimetry and Mechanism in the Hypersonic Near Wake of a MultiPurpose Crew Vehicle

5a. CONTRACT NUMBER

5b. GRANT NUMBER

5c. PROGRAM ELEMENT NUMBER

6. AUTHOR(S)

Balla, R. Jeffrey

5d. PROJECT NUMBER

5e. TASK NUMBER

5f. WORK UNIT NUMBER

478076.07.27.07

7. PERFORMING ORGANIZATION NAME(S) AND ADDRESS(ES)

NASA Langley Research Center
Hampton, VA 23681-2199

8. PERFORMING ORGANIZATION REPORT NUMBER

L-20303

9. SPONSORING/MONITORING AGENCY NAME(S) AND ADDRESS(ES)

National Aeronautics and Space Administration
Washington, DC 20546-0001

10. SPONSOR/MONITOR'S ACRONYM(S)

NASA

11. SPONSOR/MONITOR'S REPORT NUMBER(S)

NASA/TM-2013-218027

12. DISTRIBUTION/AVAILABILITY STATEMENT

Unclassified - Unlimited
Subject Category 74
Availability: NASA CASI (443) 757-5802

13. SUPPLEMENTARY NOTES

14. ABSTRACT

This study demonstrates a new molecular tagging velocimetry(MTV) method for velocity measurements of high speed flow. It demonstrates offbody Iodine Tagging Velocimetry (ITV) in the hypersonic near wake of a MultiPurpose Crew Vehicle(MPCV) model. Experiments are performed in the NASA-Langley 31-inch Mach 10 air wind tunnel. A 0.5% I2 / N2 mixture is seeded on the leeward backshell of the model using a pressure tap. I2 laser-induced fluorescence is excited along a 5.5 mm line using an ArF excimer laser near 193 nm. Results indicate I2 absorbs at least 2 photons to produce iodine ions and electrons. These recombine as the tagged region is displaced downstream to produce I (2P3/2) whose emission is monitored at 206 nm. Results at P0 = 2.41 MPa (350 psi), T0 = 990K, and 10 μsec transit times produce velocities from 630-820 m/sec across the I2 seeded jet at a distance of 38.2 mm (25.5 jet diameters) downstream from the jet orifice. Maximum wake jet velocities near the shear layer are 59% of freestream velocity.

15. SUBJECT TERMS

Hypersonic speed; Iodine tagging velocimetry; Velocity measurement; Wake measurement

16. SECURITY CLASSIFICATION OF:			17. LIMITATION OF ABSTRACT	18. NUMBER OF PAGES	19a. NAME OF RESPONSIBLE PERSON
a. REPORT	b. ABSTRACT	c. THIS PAGE			STI Help Desk (email: help@sti.nasa.gov)
					19b. TELEPHONE NUMBER *(Include area code)*
U	U	U	UU	29	(443) 757-5802